Performance Assessment of a Second-Life Li-Ion BESS for EVs Charging

Lucas A. Z. Sergio[1,2], Matheus Hohmann[1], Aline K. V. de Oliveira[1] Giuliano Luchetta Martins[2], Helena Flávia Naspolini[1] and Ricardo Rüther[1]

[1] FOTOVOLTAICA/UFSC Laboratory, Florianopolis (Brazil)

[2] Statkraft UK - London (England – United Kingdom)

Abstract

This study presents the performance assessment of a second-life Li-ion Battery Energy Storage System (BESS) used in a real-world solar carport for electric vehicle (EV) charging. The system repurposes lithium-ion modules from 2012 Nissan Leaf vehicles, with State of Health (SoH) between 60% and 75%. While IEC 62933-2-1 provides standardized procedures for controlled performance testing, this study proposes a complementary method that identifies valid cycles from regular system operation, avoiding interruptions and better reflecting the BESS usage. Key performance indicators such as DC-side Round-Trip Efficiency (RTE), Depth of Discharge (DoD), and voltage difference among cells were analysed. Preliminary results from 113 EV charges show over 2.18 MWh provided to electric cars, with 80% sourced from PV and battery. This paper provides practical insights into second-life Li-ion batteries (SLBs) performance and testing under realistic conditions.

Keywords: Battery Energy Storage System (BESS), Second-life batteries, Performance Assessment

Introduction

The accelerated adoption of electric vehicles (EVs) is expected to generate a growing volume of end-of-life lithium-ion batteries in the coming years. Once these batteries reach a usable capacity below roughly 70–80% of their original value, they are typically retired from automotive service even though they often remain functional and can be repurposed for less demanding stationary applications (IEA, 2024; Hu et al., 2022). Reusing these batteries in stationary energy storage systems—commonly referred to as second-life batteries (SLBs)—has emerged as a promising strategy to reduce costs, extend battery lifecycles, and mitigate environmental impact (Sengör & Hayes, 2024; Zago Cantú et al., 2022). Additionally, SLBs can act as effective energy buffers for EV charging, especially in areas with weak grid infrastructure or remote locations where grid access is constrained.

Despite their potential, deploying SLBs presents several technical and operational challenges. These include increased internal resistance and its evolution over time, cell voltage dispersion, heterogeneous degradation histories, and limited compatibility with commercial power electronics and Battery Management Systems (BMS) (Song H. et al., 2024; Patel et al., 2024). System-level performance metrics—such as DC-side round-trip efficiency (RTE), state of health (SoH) evolution, depth of discharge (DoD) utilization, and intra-string voltage differences—must be analyzed rigorously to ensure long-term reliability. Standardized laboratory protocols (e.g., IEC 62933-2-1 test sequences) typically rely on controlled cycling and dedicated downtime. While valuable for baseline characterization, they may be impractical for commercial assets required to remain continuously available; moreover, they can under-represent auxiliary consumption, partial cycling patterns, balancing behaviour, and parasitic standby loads. Alternative approaches based on real-world operational data can mitigate these issues while maintaining uninterrupted service.

This study proposes a non-intrusive, data-driven assessment of a second-life Battery Energy Storage System (BESS) operating within a functional solar carport used for everyday EV charging. The installation is located in Florianopolis, Brazil, and was commissioned in December 2023; the analysis covers continuous operation through October 2025. Over this period the system supported approximately 200 EV charging sessions and delivered about 3.84 MWh (AC) to the vehicle load. The carport integrates an 11 kWp photovoltaic (PV) array

10.18086/swc.2025.06.26 Available at http://proceedings.ises.org

with a single-phase 8 kW Deye hybrid inverter (220 V) and a repurposed battery bank assembled from 2012 Nissan Leaf modules (LMO chemistry). The battery is configured electrically as 7 modules in series by 8 in parallel (7s×8p). Each Leaf module consists of a 2s2p pouch-cell configuration, resulting in 14 effective series cell groups at pack level. Nominal pack ratings are 53.2 V, 528 Ah, and 28.1 kWh. A custom BMS with passive balancing, eight temperature sensors, and cell-level voltage monitoring governs safety and balancing functions; typical standby parasitic consumption (BMS plus relays) is approximately 20 W.

Operational control follows a PV-priority dispatch strategy: PV generation first supplies the EV charger (7.4 kW nominal), surplus PV charges the BESS, the BESS discharges to support EV charging during PV deficits, and limited grid top-up is permitted after 21:00 when daytime charge was insufficient. This naturally produces partial cycles, variable ramp rates, and mixed operating states that differ from standardized laboratory test conditions. These characteristics provide an opportunity to extract meaningful in-situ performance indicators that reflect real usage constraints and economic/availability priorities.

The objectives of this work are to quantify, directly from field operation logs: (i) DC-side round-trip efficiency under naturally occurring charge/discharge windows; (ii) usable energy and DoD per valid session; (iii) cell-voltage dispersion and balancing dynamics across the 14 series groups; and (iv) internal resistance / DCIR trends inferred from routine load and PV power steps, together with their relationship to apparent SoH. All metrics are computed while explicitly accounting for auxiliary and idle consumption to avoid overstating efficiency or usable capacity.

The main contributions are:

1- a practical methodology to identify and segment valid cycles from routine, non-intrusive operational data;

2- quantified performance of a 28.1 kWh second-life pack in a PV-coupled carport, including a preliminary average DC-side RTE of approximately 70.8% across accepted sessions; and

3- operational insights for improving efficiency through refined control, balancing policies, and potential strategies to reduce parasitic standby losses. By grounding analysis in real operational data rather than imposed laboratory cycling, the approach aims to reveal the true functional potential and constraints of second-life batteries deployed in distributed energy applications.

The evaluated installation is a Li-ion stationary Battery Energy Storage System (BESS) integrated into a solar carport supplying a single-phase AC EV charger in a hybrid PV-grid configuration. The battery bank consists of 56 second-life 2012 Nissan Leaf modules (LMO chemistry), screened prior to integration to ensure remaining usable capacity in the ~60–85% window (Hohmann et al., 2022; Zanicoski Sergio et al., 2024). The inverter is rated 8 kW (single-phase), and the EVSE is a 7.4 kW Type-2 unit.

1. Methodology

2.1 System Description

The UFSC Solar and Battery Carport Charging System is located in Florianópolis, Brazil. The system was commissioned at the end of December 2023, and this assessment covers continuous operation through October 2025. Some similar experimental hybrid PV–BESS have been implemented internationally to evaluate the operational feasibility of second-life battery systems under real-world charging demands (Neigum et al., 2024).

The solar system (PV) has 11 kWp array (PowerMax Strong 120 Wp modules; ≈11.2% module efficiency) on a 6° west-facing metal roof, connected to a Deye 8 kW hybrid inverter (single-phase, 220 V).

The battery system has a pack topology of 7s8p, totalizing 56 battery modules from two Nissan Leaf cars. Each Leaf module is 2s2p pouch cells monitored at cell level by the BMS. The nominal datasheet of the battery system is 53.2 V, 528 Ah, ~28.1 kWh. Before installation the modules were tested, and the SoH distribution was approximately 60–75%, consistent with the recommended thresholds for repurposing lithium-ion traction batteries (Song H. et al., 2024; Patel et al., 2024).

The custom BMS has passive balancing, eight temperature sensors (cells and ambient), cell-group voltage monitoring, and protective controls. The maximum and minimum allowed module voltages are 8.10 V and

6.60 V, defined by the manufacture (EVPV) considering battery chemistry (LMO). The passive balancing is triggered at an adjustable threshold; its configuration is refined during the project to minimize sustained dispersion. The BMS plus DC contactors remain energized continuously by the main DC buss bar from the battery, imposing a parasitic load ≈20 W that is included implicitly in energy accounting and round-trip efficiency (RTE) calculations.

For data monitoring and acquisition a Raspberry Pi 4 is used to collect inverter and BMS signals at 1 second resolution (rolling retention ≈7 days). At the main server we store 1-minute aggregates all the data collected by the Raspberry including: Cell-group voltages (14 cells), pack voltage/current, PV power, grid, and EV charging power.

Regarding the system energy flow, the battery energy is reserved for EV charging; surplus PV first charges the BESS then exports to grid once the system reaches upper SOC/Voltage limits. Night grid top-up occurs only if target SOC was not achieved during daylight.

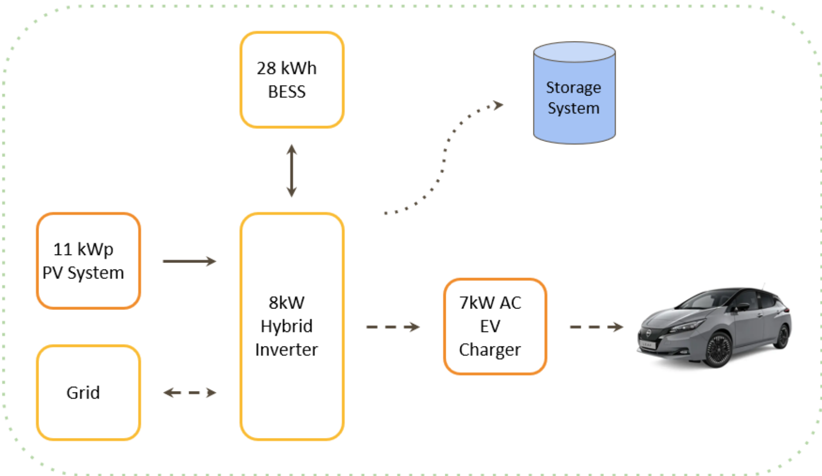

Figure 1. System block diagram (PV array, hybrid inverter, grid interface, BESS, EVSE).

2.2 Operational Control Strategy

Control prioritizes direct PV to EV supply. When instantaneous PV exceeds EV demand, surplus charges the BESS; any remaining excess is exported to the grid. During PV deficits (cloud events or evening sessions) the BESS discharges to support EV charging, if the battery is not enough finally the grid energy is used to complement the session. After the sunsets, between 19:00 and 21:00 the battery is not charged with grid energy due to the peak-price hours. At 21:00, if necessary, the battery is charged to allow morning availability of the system. This strategy produces partial, irregular cycles capturing realistic parasitic loads, balancing phases, and idle intervals. The BMS and Inverter do not communicate with each other, being necessary conservative lower voltage cutoffs, at system level, helping limit deep excursion of the most degraded modules and reducing the possibility of an emergency contactor's opening by the BMS. The study of Uwineza et al. (2022) presents a more comprehensive optimization of second-life BESS control; however, due to the specific operational and availability requirements of this project, a custom charge/discharge strategy was developed.

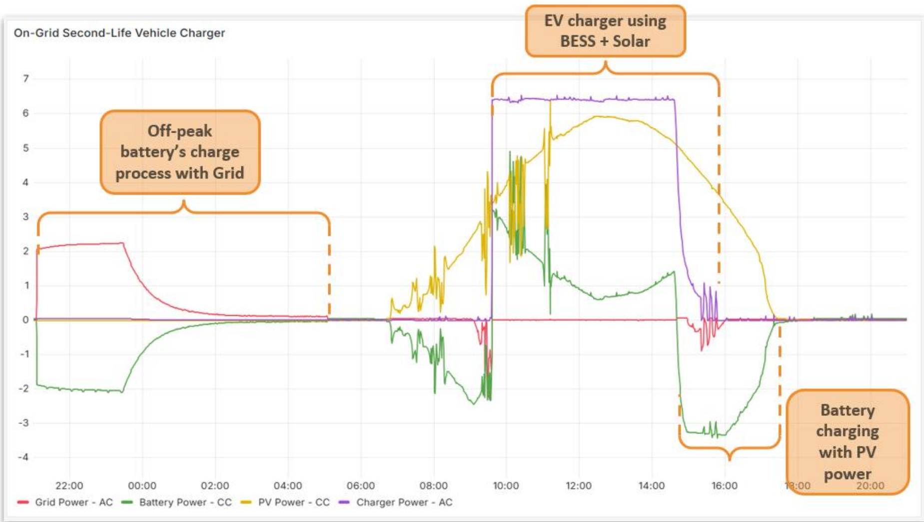

Figure 2. Example 24 h power-flow (PV, BESS, Grid, EV) illustrating PV and BESS priority. Vertical axis representing power in KW.

2.3 Data Acquisition & Pre-Processing

To ensure robust data acquisition and pre-processing, the system continuously monitors the signals, including pack voltage and current, voltages across 14 individual cell groups, PV power, grid import and export data and EV charging power. Data is initially captured at a high temporal resolution of one second, with subsequent aggregation to one-minute intervals due to storage and process limitation. Data from the inverter and battery management system (BMS) are synchronized using an "inner" join, ensuring that only periods with available data from both systems are retained. If either subsystem has missing data at a particular timestamp, that timestamp is excluded from analysis to ensure consistent temporal alignment across datasets.

Also, filtering procedures are applied to remove invalid records, such as missing values (NaNs) at none index columns, frozen sensor readings, and voltage spikes, while plausible operational bounds are fulfilled, specifically, pack voltages are constrained between 46 V and 60 V, currents are limited to inverter specifications, and cell-group voltages are maintained within defined safety ranges. For all measurements, the sign convention adopted is positive current for discharging ($I > 0$ A) and negative current for charging ($I < 0$ A), facilitating consistent interpretation throughout the analysis.

2.4 Cycle Identification

The international standard IEC 62933-2-1 (International Electrotechnical Commission, 2017) establishes performance test procedures for stationary energy-storage systems under controlled laboratory conditions. According to the standard, efficiency and capacity measurements must be performed through full and consecutive charge-discharge cycles executed at constant current or power, with the system isolated from external loads and environmental variability. Although this ensures repeatability, it requires complete suspension of normal operation and may not represent the complex, partial-cycling behaviour of real-world systems.

To address this limitation, the present work employs a non-intrusive cycle-identification methodology that reconstructs valid cycles directly from day-to-day operational data. This approach preserves normal functionality while enabling statistically robust estimation of Round-Trip Efficiency (RTE), Depth of Discharge (DoD), and other key indicators.

The procedure is summarised below.

1- **Segmentation by current sign.**

The one-minute time-series of pack current is classified into three states: charge ($I<0$ A), discharge ($I>0$), and idle ($|I|<I_{idle}|$). where $I_{idle} = 1$ A defines the noise threshold.

2- **Merging of micro-segments.**

Adjacent segments separated by short gaps (≤ 2–5 min) are merged to compensate for transient measurement interruptions or brief current reversals due to inverter control.

3- **Energy validation.**

Each segment's energy throughput is obtained by integrating pack power $P(t)=V_{pack}(t)I_{pack}(t)$ over time. Segments delivering less than 10 kWh (≈ 35% DoD) or showing incomplete telemetry are discarded to suppress micro-events and noise.

4- **Cycle pairing.**

The remaining segments are paired chronologically, linking each charge event to the subsequent discharge event occurring after an idle interval of at most 8 h. Each pair constitutes one valid cycle.

5- **KPIs.**

For every valid cycle, the following quantities are derived on the DC side: Discharged Energy, Charged Energy, RTE and DoD.

6- **Inclusion of auxiliary and idle losses.**

No trimming is applied between charge and discharge intervals; therefore, auxiliary loads (BMS, contactors, balancing) and idle self-consumption remain included. The resulting RTE thus represents the operational efficiency of the system under realistic availability conditions rather than the idealised efficiency defined by IEC tests.

This methodology allows the determination of an effective number of cycles during the analysed period while preserving normal daily operation. By combining continuous monitoring with statistical filtering, it provides a faithful representation of the system's long-term field performance and complements the controlled-test approach prescribed by IEC 62933-2-1.

2.5 Key Performance Indicators (KPIs)

Unless otherwise stated, all key performance indicators (KPIs) are computed on the DC side of the battery using time-aligned measurements of pack voltage $V_{pack}(t)$, pack current $I_{pack}(t)$, and, where applicable, cell-group voltages $V_i(t)$. The sign convention adopted throughout is $I>0$ for discharging and $I<0$ for charging, consistent with ESS performance protocols (PNNL, 2016; IEC, 2017).

Instantaneous pack power:

$$P_{\text{pack}}(t) = V_{\text{pack}}(t) * I_{\text{pack}}(t), \qquad \text{(eq. 1)}$$

So $P_{pack}(t) > 0$ during discharge and $P_{pack}(t) < 0$ during charge.

Segment energies (charge / discharge): To avoid sign ambiguity, energies are defined as non-negative magnitudes over each segment:

$$E_{\text{chg}} = \int_{\text{charge}} |P_{\text{pack}}(t)|\, dt, \qquad \text{(eq. 2)}$$

$$E_{\text{dis}} = \int_{\text{discharge}} |P_{\text{pack}}(t)|\, dt. \qquad \text{(eq. 3)}$$

With the adopted convention, $P_{pack}<0$ on charge.

Round-Trip Efficiency (RTE): For each valid paired cycle identified in Section 2.4,

$$RTE\ (\%) = \left(\frac{E_{Discharge}}{E_{Charge}}\right) * 100 \qquad \text{(eq. 4)}$$

No trimming is applied between segments; thus, auxiliary and idle consumptions (BMS, contactors, balancing, standby) remain included, yielding an operational rather than idealized efficiency.

Depth of Discharge (DoD):

$$DoD\ (\%) = \left(\frac{E_{Discharge}}{E_{Nominal}}\right) * 100 \qquad \text{(eq. 5)}$$

$$E_{nom} = V_{nom} * C_{nom} \qquad \text{(eq. 6)}$$

Using pack ratings V_{nom}=53.2 V and C_{nom}=528 Ah, E_{nom}≈28.1 kWh. DoD and capacity expressions are consistent with IEC 62660-1 (2018).

Capacity and State of Health (SoH): When near-full, constant-current discharges are present, the delivered capacity is:

$$C_{meas} = \int_{\text{discharge}} I_{\text{pack}}(t)\, dt, \qquad \text{(eq. 7)}$$

$$SoH\ (\%) = \frac{C_{meas}}{C_{nom}} * 100, \qquad \text{(eq. 8)}$$

Otherwise, SoH is tracked via a DCIR-based proxy (non-intrusive trend only), following the methodology proposed by Hohmann, Matheus (2022) for second-life lithium-ion systems.

$$SoH\ (\%) = -6.2982 * DCIR + 110.15. \qquad \text{(eq. 9)}$$

Energy-flow: To characterise operating modes and seasonal effects, cumulative energy transfers are accrued from metered streams: PV→EV, BESS→VE, Grid→BESS and Grid→EV.

DC Internal Resistance (DCIR) Estimation

To estimate DC internal resistance under routine operation, we compute DCIR from short, natural load transitions observed in the synchronized time series. Measurements include pack voltage $V_{pack}(t)$, pack current $I_{pack}(t)$, and voltages of 14 series cell-groups $V_i(t)$ (Nissan LEAF modules, 2s2p taps). This non-intrusive approach follows methodologies successfully applied in field characterization of EV and stationary lithium-ion systems (AOKI et al., 2021).

Operating window and current gate: To avoid edge-SOC polarization and ensure a quasi-linear region, analysis is restricted to 3.80–3.95 V per cell (≈ 53.2–55.3 V for 14 V_{pack}). Only high-confidence discharge samples are considered using a minimum value of 115 A (≈ C/5 for a 528 Ah pack), which ensures a measurable voltage drop while limiting electrochemical relaxation effects (Li et al., 2022).

Event detection and signal-quality filters: DCIR is computed across small, naturally occurring current increments (“steps”) detected in the EV charger system. To suppress numerical amplification of noise in the finite-difference ratio ΔV/ΔI, we apply the following filters:

Minimum step amplitude: |ΔI| ≥ 5 A between consecutive samples (or between short moving-average points).

Voltage boundaries: per-cell voltages remain within the [3.80, 3.95] V window; pack voltage within the corresponding 53.2–55.3 V bounds.

Outlier control: we retain only values up to the 75th percentile of the provisional DCIR distribution (i.e., discard the top-tail transients that typically arise from brief controller actions or measurement jitter).

These criteria reject low-signal steps and noisy transients while preserving physically consistent events in the linear region.

Finite-difference DCIR computation: Let t and t+Δt denote adjacent analysis instants (or the centres of short pre/post averaging windows). The pack-level DCIR is given by:

$$DCIR_{pack} = \left| \frac{V_{pack}(t+\Delta t) - V_{pack}(t)}{I_{pack}(t+\Delta t) - I_{pack}(t)} \right|. \qquad \text{(eq. 10)}$$

Analogously, the cell-group DCIR for each cell *i* is:

$$DCIR_i = \left| \frac{V_i(t+\Delta t) - V_i(t)}{I_i(t+\Delta t) - I_i(t)} \right|. \qquad \text{(eq. 11)}$$

Internal vs. external (cable) resistance: The sum of cell-group resistances approximates the internal series resistance of the battery system:

$$DCIR_{\sum cells} = \sum_{i=1}^{14} DCIR_i. \qquad \text{(eq. 12)}$$

Assuming a series topology, the additional DC resistance attributable to busbars, cabling, and interfaces between the pack and the inverter is then:

$$DCIR_{cable} = DCIR_{pack} - DCIR_{\sum cells}. \qquad \text{(eq. 13)}$$

2. Results

3.1 Energy Flow Analysis

A total of 205 EV charging cycles were recorded since the commissioning of the project. During this period, the system delivered 3.94 MWh of energy to the electric vehicles. Figure 3 summarizes the overall energy flow, 1.64 MWh supplied directly from the PV system, 1.39 MWh supplied by the second-life BESS and 1 MWh imported from the grid.

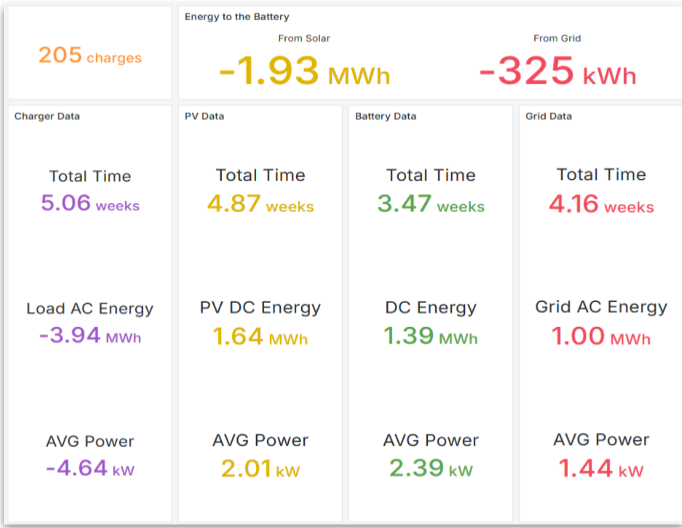

Figure 3. Cumulative energy-flow distribution of the system.

To recharge the battery bank, 1.93 MWh were sourced from PV and only 325 kWh from the grid, highlighting the strong contribution of on-site renewable generation.

This distribution demonstrates that the BESS played a significant role in enabling energy autonomy and availability strategy. It also establishes a solid baseline for subsequent performance evaluation metrics such as RTE, DoD and SOH.

3.2 Round-Trip Efficiency (RTE)

After applying quality filters to the dataset, 43 valid cycles remained for the RTE calculation. The average RTE observed was 72.3%, as illustrated in Figure. 4.

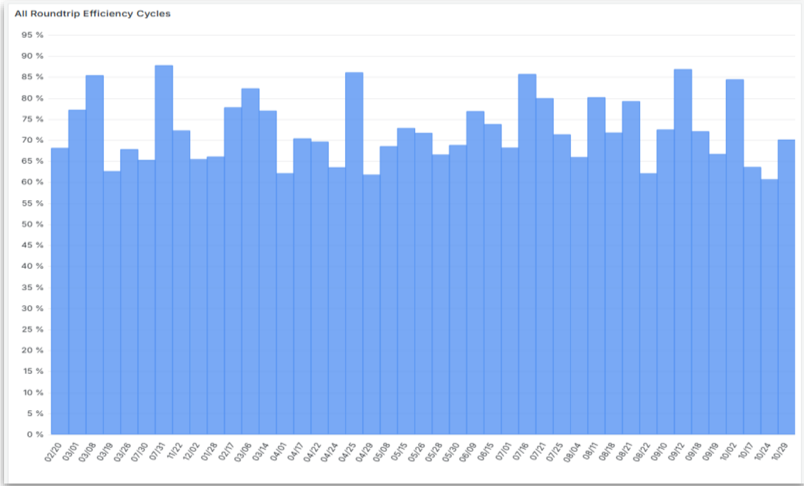

Figure 4. Round-Trip Efficiency (RTE) for all valid charging/discharging sessions.

While expected to be lower than first-life systems, an RTE of ~72% is still relatively low, even for second-life configurations. Investigation of the DC bus revealed the presence of constant parasitic losses in the battery architecture. Two components were identified as sources of continuous consumption:

1. The BMS powered directly from the DC bus, and
2. A DC safety contactor permanently energized.

Together, these components draw approximately 40 W at all times, resulting in a sustained voltage drop clearly visible in Figure. 5.

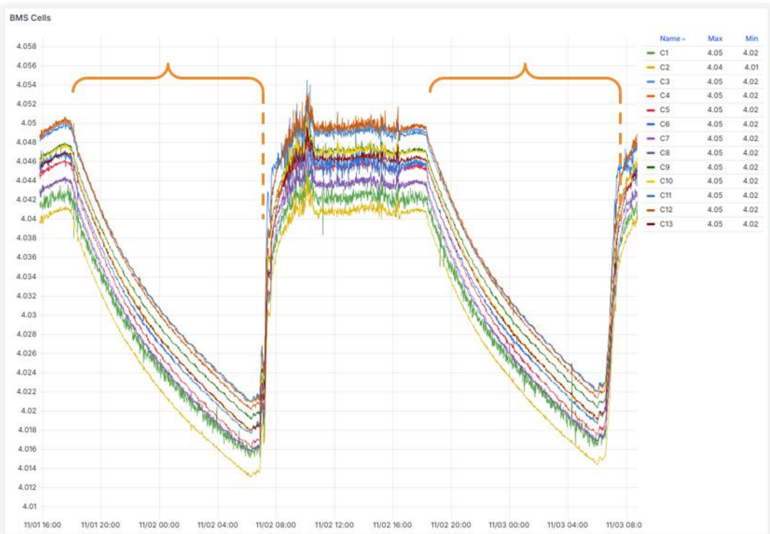

Figure 5. Cell's voltage behaviour indicating constant parasitic consumption of approximately 40 W caused by the BMS and DC safety contactor. Vertical axis representing voltage in V.

These parasitic loads significantly impact the effective usable energy of the pack and directly contribute to the reduced RTE.

3.3 Depth of Discharge (DoD)

As expected at a battery system, the usable Depth of Discharge is limited by the weakest cell. For this project, the average DoD observed across all valid cycles was 44%, which corresponds to approximately 12.4 kWh of usable energy, based on the nominal new capacity of 28.1 kWh.

Given that the system provided access to individual cell voltage measurements, it was possible to investigate the root cause of the limited DoD. The voltage–time profiles (Figure. 6) revealed that several cells consistently reached the lower safety cutoff before the majority of the pack.

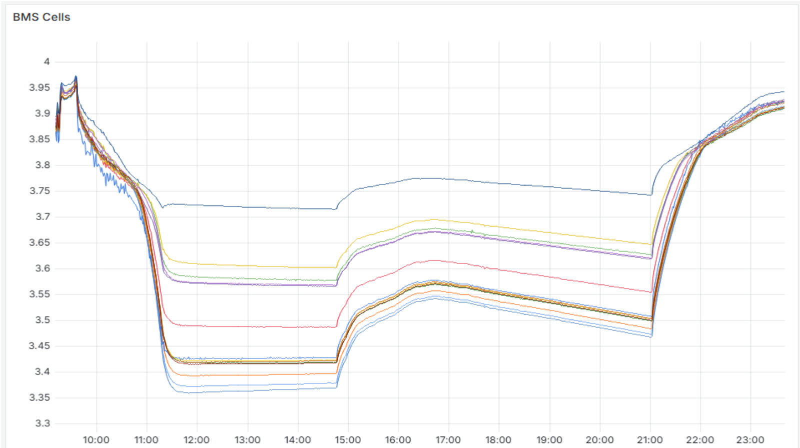

Figure 6. Example of individual cell-voltage profile during a discharge event. Vertical axis representing voltage in V.

This behaviour is indicative of capacity imbalance, which is common in second-life modules due to heterogeneous aging histories. These weak cells prematurely trigger the BMS low-voltage protection, effectively limiting the available energy window of the entire pack and ultimately contributing to the lower-than-expected DoD.

3.4 DC Internal Resistance (DCIR)

The internal resistance of each cell was calculated using the methodology described previously. The average cell-level DCIR was found to be 6.4 mΩ.

At the inverter level, however, the calculated DCIR for the same operating period was 100 mΩ. By subtracting the cell contribution, it is possible to estimate that the DC wiring and auxiliary circuit resistance account for approximately 93.5 mΩ.

This discrepancy indicates a significant portion of losses occurring outside the cell chemistry itself, suggesting that cable sizing and overall pack architecture optimization could lead to meaningful improvements in system efficiency.

3.5 State of Health (SOH) and Degradation Rate

Using the SOH estimation approach described in Section 2.5, the average SOH during the first two months of operation was 69.74%. In contrast, the most recent two months showed a reduced average SOH of 59.43%.

Using the 75th percentile points extracted from the SOH distribution (Figure. 7), a clear downward trend was observed. From this regression, we estimate an overall degradation of approximately 10.31% across all 205 EV charging cycles.

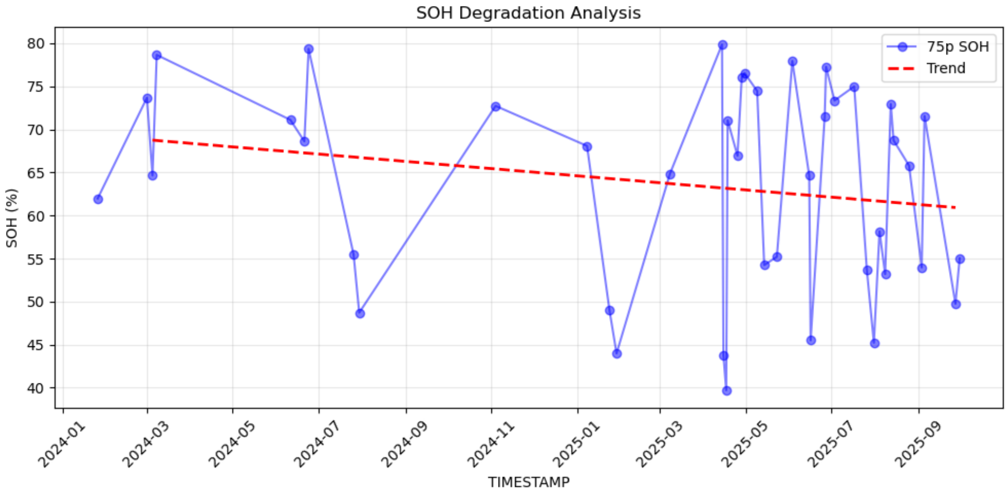

Figure 7. State of Health (SOH) estimates over the project evaluation period.

This corresponds to a degradation rate of ≈0.05% per cycle. The combination of high DoD, for a 2nd life BESS, operation and parasitic losses may have influenced the apparent SOH evolution, emphasizing once again that both electrical and architectural factors shape the effective degradation path.

3. Conclusion

This study presented a real-world performance assessment of a second-life lithium-ion battery system used for EV charging support in a hybrid PV–BESS–Grid environment. The adapted methodology, based on energy-flow monitoring, cell-level voltage analysis, DCIR estimation, and session-by-session KPI extraction, proved effective for identifying operational behaviour and degradation patterns under practical conditions. The results confirmed that the system consistently supported all EV charging events while maintaining low dependence on grid import, demonstrating the technical feasibility of repurposing retired traction batteries for stationary applications.

Across 205 EV charging cycles, the system delivered 3.9 MWh to vehicles, with a significant portion supplied by PV generation and the second-life BESS. Despite the limited Depth of Discharge imposed by weaker cells within the pack, the battery operated predictably, with DoD values centered around 44% and with a stable SOH trajectory. The observed degradation of approximately 10.31% over the evaluation period—equivalent to 0.05% per cycle—aligns with reported values for similar second-life deployments, confirming that the system exhibits realistic and expected aging behaviour for modules with heterogeneous first-life histories.

The average Round-Trip Efficiency of 72.3%, although within the lower range for second-life systems, was strongly impacted by parasitic loads introduced by the BMS and DC safety contactor, which together consumed approximately 40 W continuously. This finding highlights the importance of architectural decisions in repurposed systems: auxiliary components can represent a significant portion of losses, especially in shallow-cycle applications. Similarly, the discrepancy between cell-level DCIR (6.4 mΩ) and inverter-level DCIR (100 mΩ) revealed substantial contributions from wiring and external components, emphasizing the role of pack layout and cabling optimization in improving overall efficiency.

From a practical standpoint, two areas were identified for improvement: reducing parasitic losses to enhance RTE and rearranging the modules to achieve better pack balance and increase usable DoD. The KPIs calculated in this study provide a valuable benchmark for comparing real-world second-life system behaviour against international standards such as IEC 62660 and IEC 62933. By aligning future assessments with such standards, it becomes possible to harmonize repurposing criteria and support the broader adoption of second-life batteries in distributed energy applications.

Overall, the results demonstrate that second-life lithium-ion batteries can deliver stable performance, predictable degradation, and meaningful energy autonomy when properly integrated into hybrid energy systems. The insights presented here contribute to the development of more efficient, reliable, and cost-effective second-life deployments, supporting the transition toward a circular economy in energy storage. Future work may include long-term cycling studies, automated cell classification methods, and model-based or data-driven SOH prediction approaches to further refine diagnostic tools for repurposed battery systems.

4. Acknowledgments

The authors express their sincere gratitude to the Conselho Nacional de Desenvolvimento Científico e Tecnológico (CNPq – Project: 406361/2022-3) for the financial support. This research was also carried out within the scope of the activities of the National Institute for Technological Development of Photovoltaic Solar Energy Applications (INCT-DAESF, CNPq/MCTI/Brazil, Process 408486/2024-4).

5. References

International Energy Agency – IEA. (2024). Global EV *Outlook 2024: Scaling up the transition to electric mobility*. Paris: IEA.

Hu, X., Xu, L., Lin, X., Pecht, M., & Zhang, L. (2022). *Battery second use: Present status, challenges, and future prospects. Renewable and Sustainable Energy Reviews*, 154, 111890. https://doi.org/10.1016/j.rser.2021.111890

Sengör, M., & Hayes, J. (2024). *Circular economy opportunities in second-life EV batteries for stationary applications. Energy Storage Materials*, 66, 123–139.

Zago Cantú, A., Kim, J., & Park, C. (2022). *Sustainability assessment of second-life battery applications: Technical and environmental perspectives*. Journal of Energy Storage, 55, 105947.

Hohmann, M., Naspolini, H. F., Sergio, L. A. Z., Oliveira, A. K. V. de, Pacheco, L. F., & Rüther, R. (2024). *Avaliação de métodos para caracterização de baterias de lítio em segunda vida. Anais Congresso Brasileiro de Energia Solar – CBENS.* https://doi.org/10.59627/cbens.2024.2446

Zanicoski Sergio, L. A., & Hohmann, M. (2024). *Performance modeling of hybrid PV–BESS carports for electric vehicle charging applications. Renewable Energy Research Journal, 19*(3), 210–224.

Kim, H., & Lee, J. (2023). *Real-world operational data analytics for second-life battery performance evaluation. IEEE Transactions on Energy Conversion, 38*(5), 4412–4423.

Neigum, K., Smith, J. L., & Toghrol, M. (2024). *Technology, economic, and environmental analysis of second-life lithium-ion batteries for energy storage systems. Sustainable Energy Technologies and Assessments*, 63, 103276. 10.1016/j.est.2024.114393

Song, H., Zhang, Z., & Li, K. (2024). *An overview about second-life battery utilization for stationary applications*. Energies, 17(23), 6163. https://doi.org/10.3390/en17236163

Uwineza, L., Park, C., & Lee, H. (2022). *Technical control and optimal dispatch strategy for a hybrid photovoltaic–battery energy storage system*. Energies, 15(8), 2744. https://doi.org/10.3390/en15082744

International Electrotechnical Commission (IEC). (2017). *IEC 62933-2-1: Electrical energy storage (EES) systems – Part 2-1: Unit parameters and testing methods – General specification*. Geneva: IEC.

Hohmann, Matheus. 2022. *Avaliação de métodos para a caracterização de baterias de lítio em segunda vida*. Universidade Federal de Santa Catarina. Repositório UFSC. https://repositorio.ufsc.br/handle/123456789/240435

AOKI, Tatsuya & MATSUYAMA, Tetsuya & Miyata, Kikuko & Tsuruda, Yoshihiro & Yamagata, Masaki. (2021). Internal resistance of commercial lithium-ion battery evaluated by current-rest-method and its application to on-orbit charge/discharge simulation for microsatellites.. The Proceedings of Mechanical Engineering Congress Japan. 2021. J191-13. 10.1299/jsmemecj.2021.J191-13.

Li, Y., Diao, W., & Wu, C. (2022). *On-line estimation of internal resistance and power capability of lithium-ion batteries using current pulse features. Journal of Energy Storage, 49,* 104078. https://ieeexplore.ieee.org/stamp/stamp.jsp?arnumber=10857323